D.R. OLIINYCHENKO,[1] K.A. BUGAEV,[2] A.S. SORIN[1]

[1] Bogoliubov Laboratory of Theoretical Physics
(6, Joliot-Curie Str., JINR, Dubna 141980, Russia; e-mail: dimafopf@gmail.com, Sorin@theor.jinr.ru)

[2] Bogolyubov Institute for Theoretical Physics, Nat. Acad. of Sci. of Ukraine
(14b, Metrolohichna Str., Kyiv 03680, Ukraine; e-mail: bugaev@th.physik.uni-frankfurt.de)

INVESTIGATION OF HADRON MULTIPLICITIES AND HADRON YIELD RATIOS IN HEAVY ION COLLISIONS

PACS 25.75.-q, 25.75.Nq

We thoroughly discuss some weak points of the thermal model, which is traditionally used to describe the hadron multiplicities measured in the central nucleus-nucleus collisions. In particularly, the role of conservation laws and the values of hard-core radii along with the effects of the Lorentz contraction of hadron eigenvolumes and the hadronic surface tension are systematically studied. It is shown that, for the adequate description of hadron multiplicities, the conservation laws should be modified, whereas the conservation laws are not necessary at all for the description of hadron yield ratios. We analyzed the usual criteria for the chemical freeze-out and found that none of them is robust. A new chemical freeze-out criterion of constant entropy per hadron equals to 7.18 is suggested, and a novel effect of adiabatic chemical hadron production is discussed. Additionally, we found that the data for the center-of-mass energies above 10 GeV lead to the temperature of the nil hadronic surface tension coefficient of about $T_0 = 147 \pm 7$ MeV. This is a very intriguing result, since a very close estimate for such a temperature was obtained recently within an entirely different approach. We argue that these two independently obtained results evidence that the (tri)critical temperature of a QCD phase diagram is between 140 and 154 MeV. In addition, we suggest to consider the pion and kaon hard-core radii as new fitting parameters. Such an approach allows us, for the first time, to simultaneously describe the hadron multiplicities and the Strangeness Horn and to get a high-quality fit of the available experimental data.

K e y w o r d s: hadron resonance gas, second virial coefficients, chemical freeze-out

1. Introduction

Experimental data on heavy ion collisions have traditionally been described by the thermal model [1–27]. The thermal model core assumption is that the fireball produced in the relativistic nuclear collision reaches thermodynamic equilibrium. Such an assumption allows one to describe the multiplicities of particles registered in the experiment using two parameters, namely the temperature T and the baryochemical potential μ_b. The extracted values of T and μ_b not only describe the experimental data, but they also give an essential information about the last stage of fireball evolution, when the inelastic collisions cease to exist, but the elastic collisions between hadrons and the decay of resonances take place. This stage is usually called the chemical freeze-out. The thermal model was initially used for the AGS and SPS data [13] and was subsequently employed to describe the data collected at SIS [14,15], SPS [16], and RHIC [17–

20]. Using the thermal model, it was possible to correctly predict the hadron ratios measured at LHC [2], while the only wrong prediction for LHC was made for $\bar{p}/\pi^-$ ratio [21]. An analysis of the energy dependence of thermal parameters extracted from fits of the experimental data established the line of chemical freeze-out [22]. Consequently, the thermal model is an established tool for the particle production analysis and the chemical freeze-out investigation.

However, the thermal model suffers from several weak points, which should be accounted for in more careful studies. The present paper is just devoted to a critical analysis of the thermal model and contains several directions to develop and to improve it. First of all, we would like to note that the term "thermal model" is a common name for a set of similar models, each having its specific features such as the strangeness suppression factor γ_s, the inhomogeneous freeze-out scenario [14, 19, 26, 27], *etc.* Here, we consider the minimal thermal model with two major parameters T and μ_b, following the approach of Andronic *et al.*, [2]. Below, we briefly formulate the main problems of the model to be analyzed in the present work.

– **Particle table.** In order to describe the experimental data using the thermal model, one needs the masses, widths, and decay branching ratios of all existing resonances. In principle, the mass spectrum of hadronic resonances that are heavier than 2.3 GeV is known poorly, and, hence, they could create a problem. However, it was shown recently that the large width of heavy resonances leads to their strong suppression [28], and, hence, their contribution to the thermodynamic functions of the hadronic phase is negligible.

Note that not only the parameters of hadrons from the "tail" of the mass spectrum are poorly known. For example, both the mass and the width of $\sigma(600)$ meson are not well established, but the thermal model predictions are strongly influenced by the values of the mass and width of this meson [3]. For many other baryons, the width and the branching ratios of decays are not well established at all. Thus, the particle table is one source of uncertainty of the thermal model.

– **Radii of hard-core spheres.** The ideal-gas description has proven to be unsatisfactory [4] long ago. The simplest way to introduce an interaction between hadrons is to use the repulsive hard-core potential, since the attraction between them is usually accounted for via many sorts of hadrons [28]. In the simplest case, this potential depends only on a single parameter – the hard-core radius. In the general case, each particle type can be characterized by its own hard-core radius. But, for the sake of convenience and simplicity, the hard-core radius is usually taken to be identical for all particles. The usual value for such a radius is $r = 0.3$ fm. This value is motivated by the hard-core volume known from nucleon-nucleon scattering [1]. There are, however, two restrictions on the range of hard-core radii: (i) they should be small enough to satisfy the condition $V_{\rm eigen} \ll V$, i.e. the total eigenvolume of all particles $V_{\rm eigen}$ should be much smaller than the total volume of the system, V; (ii) on the other hand, these radii should not be too small, because, otherwise, the model will lead to a contradiction with the lattice quantum chromodynamics (QCD) thermodynamics data [8]. Thus, there is a certain freedom in defining the values of hard-core radii which, so far, was not systematically exploited to describe the whole massive of existing experimental data.

– **Conservation laws.** Here, we would like to discuss the baryon charge and isospin projection conservation laws. It was suggested to use them in the form [2]

$$\begin{cases} \sum_i n_i I_{3i} = I_{3\rm init}/V, \\ \sum_i n_i B_i = B_{\rm init}/V. \end{cases}$$

The initial values are chosen $I_{3\rm init} = -20$ and $B_{\rm init} = 200$ [2], neglecting the fact that only a part of initial particles belongs to the midrapidity region. Below, we study the role of these conservation laws and show that such a treatment leads to physically unrealistic freeze-out volumes and to a very bad description of hadron multiplicities, while the description of particle yield ratios (we use such a term for the ratio of multiplicities in order to avoid a confusion) can be extremely good.

– **Multiplicities fit.** The fit of hadron multiplicities is usually performed, by using three parameters: T, μ_b, and V [2]. Below, we show that such a procedure combined with the above-mentioned conservation laws is mathematically ambiguous, and it leads to the problems with the imposed baryonic charge conservation law.

In addition to these usual features of the thermal model, we would like to thoroughly investigate the

role of the Lorentz contraction of the eigenvolumes of hadrons to essentially improve the previous analysis [24, 25, 29] and to study the influence of the hadronic surface tension on the fit of the freeze-out parameters. As we argued, the latter may provide us with a new information about the critical temperature value of the QCD phase diagram. Such a comprehensive analysis of the different features of the thermal model and the experimental data will also allow us to elucidate the correct criterion of the chemical freeze-out, which is a very hot topic nowadays. Furthermore, we perform the simultaneous fit of hadron multiplicities and the K^+/π^+ ratio for all available energies of collisions and, hence, obtain, for the first time, the high-quality fit of the Strangeness Horn, i.e., the peak of the K^+/π^+ ratio.

The work is organized as follows. The basic features of the thermal model are outlined in the next section. In Section 3, we discuss the important problems related to the conservation laws and propose their solutions. The discussion of the existing chemical freeze-out criteria and the formulation of a new criterion along with a novel effect of the adiabatic chemical hadron production are given in Section 4, while Section 5 is devoted to the model reformulation for a multicomponent hadron gas mixture. In Section 6, we investigate the values of hard-core radii and study the effect of the Lorentz contraction of hard-core spheres. Section 7 is devoted to the analysis of the hadronic surface tension, while, in Section 8, we describe the Strangeness Horn. Section 9 contains our conclusions.

2. Model Formulation

In order to study the role of conservation laws in a form suggested in [2] and employed in their subsequent publications, it is necessary, first of all, to reproduce the results obtained in that work. For this purpose, let us consider the Boltzmann gas consisting of hadrons of s sorts with temperature T and volume V. Each i-th sort is characterized by its own mass m_i and chemical potential μ_i. Suppose that the number of particles of the i-th sort is N_i. Then its canonical partition function is

$$Z_{\rm can}(T,V,N_1,\ldots,N_s) = \\ = \prod_{i=1}^{s}\left[\frac{g_i V}{(2\pi)^3}\int \exp\left(-\frac{\sqrt{k^2+m_i^2}}{T}\right)d^3k\right]^{N_i}. \quad (1)$$

Here, $g_i = 2S+1$ is the degeneracy factor of the i-th hadron sort, and k is the particle momentum. The corresponding grand canonical partition function reads

$$Z_{\rm gr.can.} = \sum_{N_1=0}^{\infty}\cdots\sum_{N_h=0}^{\infty}\exp\left[\frac{\mu_1 N_1+\cdots+\mu_s N_s}{T}\right]\times \\ \times Z_{\rm can}(T,N_1,\ldots,N_s). \quad (2)$$

From (2), one gets the number of particles of each sort:

$$N_i = V\phi_i(T,m_i,g_i)\exp\left[\frac{\mu_i}{T}\right] \equiv \\ \equiv \frac{g_i V}{(2\pi)^3}\int\exp\left(\frac{\mu_i-\sqrt{k^2+m_i^2}}{T}\right)d^3k. \quad (3)$$

Following the commonly accepted approach, we consider the conservation of baryon charge B, strangeness S, and isospin projection I_3 on the average:

$$\sum_{i=1}^{N} n_i S_i = S_{\rm init} = 0, \quad (4)$$

$$\sum_{i=1}^{N} n_i B_i = B_{\rm init}/V = 200/V, \quad (5)$$

$$\sum_{i=1}^{N} n_i I_{3i} = I_{3\rm init}/V = -20/V. \quad (6)$$

These conservation laws define the value of total chemical potential for hadrons of the sort i as $\mu_i = \\ = B_i\mu_b + S_i\mu_s + I_{3i}\mu_{I_3}$, where the quantities B_i, S_i, and I_{3i} denote, respectively, the baryonic, strange, and isospin projections of such a hadron, while the corresponding chemical potentials are denoted as μ_b, μ_s, and μ_{I_3}.

The interaction of hadrons and resonances is usually accounted for by the hard-core repulsion of the van der Waals type [5] as

$$p = p_{\rm id.gas}\exp\left(-\frac{pb}{T}\right), \quad n_i = \frac{n_i^{\rm id}\exp\left(-\frac{pb}{T}\right)}{1+\frac{pb}{T}}, \quad (7)$$

where the pressure $p_{\rm id.gas}$ and the i-th charge density $n_i^{\rm id}$ of an ideal gas is modified due to the hard-core repulsion. Here, $b = \frac{2\pi}{3}(2R)^3$ is the excluded volume for the hard-core radius R, which was taken in actual calculations to be $R = 0.3$ fm for all hadrons. The

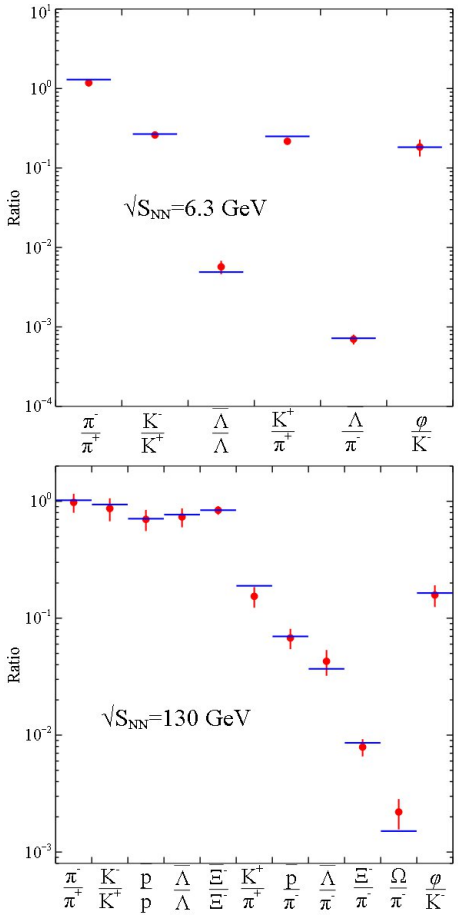

Fig. 1. Examples of the description of particle yield ratios. Dots denote the experimental values, while the lines show the fitting results. Upper panel: $\sqrt{S_{NN}} = 6.3$ GeV, $T = 139$ MeV, $\mu_b = 503$ MeV, the mean square deviation per degree of freedom is $\chi^2/NDF = 4.8/4$. Lower panel: $\sqrt{S_{NN}} = 130$ GeV, $T = 169$ MeV, $\mu_b = 31$ MeV, $\chi^2/NDF = 3.4/9$

usual van der Waals correction affects the particle densities, but has no effect on the particle ratios [5]. While its effect on the charge and particle densities may be strong, the excluded volume correction for the freeze-out densities obtained at and above the highest SPS energy $\sqrt{S_{NN}} = 17.6$ GeV leads to a reduction of the densities by about of 50 percent.

As usual, the resonance decays are accounted for in the following way: the final multiplicity of hadron X consists of the thermal contribution $N_X^{\rm th}$ and the decay ones:

$$N_X^{\rm fin} = N_X^{\rm th} + N^{\rm decay} = N_X^{\rm th} + \sum_Y N_Y^{\rm th} Br(Y \to X), \quad (8)$$

where $Br(Y \to X)$ is the decay branching of the Y-th hadron into the hadron X. The masses, widths, and decay branchings were taken from the particle tables used by the thermodynamic code THERMUS [7].

The width Γ of the resonance with mean mass m is accounted for by replacing the Boltzmann distribution function in the particle pressure by its average over the Breit–Wigner mass distribution as

$$\int \exp\left(\frac{-\sqrt{k^2+m^2}}{T}\right) d^3k \to$$

$$\to \frac{\int_{M_0}^{\infty} \frac{dx_i}{(x_i-m)^2+\Gamma^2/4} \int \exp\left(\frac{-\sqrt{k^2+x_i^2}}{T}\right) d^3k}{\int_{M_0}^{\infty} \frac{dx_i}{(x_i-m)^2+\Gamma^2/4}}, \quad (9)$$

where M_0 is the dominant decay channel threshold.

3. Role of Conservation Laws

Using the thermal model formulated in the previous section, we fitted the hadron yield ratios in the energy range from AGS to RHIC, i.e., for $\sqrt{S_{NN}} = 2.7 \div 200$ GeV. We used the χ^2 minimization for all the ratios available for this energy range as the fit criterion. The present consideration is very similar to that used in [2]. The main sources of difference are listed below.

– **The Boltzmann statistics** is used here instead of the quantum statistics employed in [2]. This allows us to essentially fasten the simulations since the momentum integration can be done only once for each hadron species. We checked that, for the freeze-out temperatures $T \geq 50$ MeV obtained here, the difference of the results due to the Boltzmann statistics is almost negligible.

– **The charm conservation** is not accounted for by the present model, since it is important only for the charmed particles multiplicities description which is not considered here.

– **The particle table** used here is slightly different from that in [2], but this does not lead to a big difference in results. Although, in contrast to [2], we do not fit the mass and the width of $\sigma(600)$ meson.

– **Inclusion of the resonance width** is done in this work for all values of colliding energy $\sqrt{S_{NN}}$, while the width was accounted in [2] only for the AGS energy range.

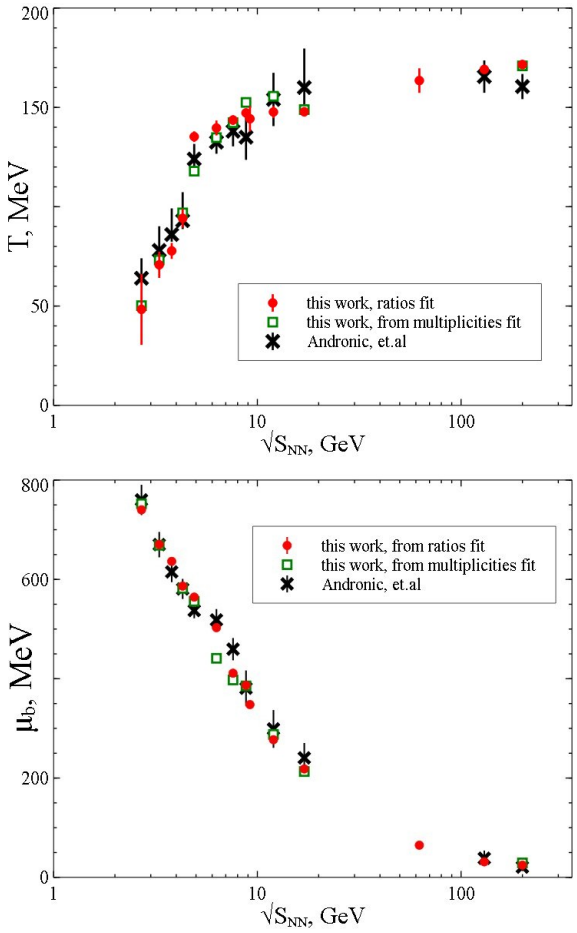

Fig. 2. Dependence of thermal model fitting parameters on the center-of-mass collision energy $\sqrt{S_{NN}}$. Upper panel: the chemical freeze-out temperature T vs. $\sqrt{S_{NN}}$. Lower panel: the chemical freeze-out baryonic chemical potential μ_b vs. $\sqrt{S_{NN}}$. The results obtained from the fit of hadron yield ratios (circles) with the conservation laws and from the fit of hadron multiplicities (open squares) are compared with those obtained in [2] (crosses)

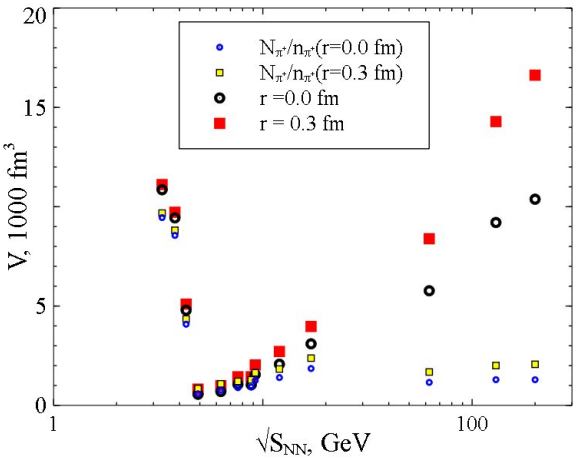

Fig. 3. Chemical freeze-out volume vs. $\sqrt{S_{NN}}$ for the ideal hadron gas and the hadron gas with hard-core radii of 0.3 fm. The smaller symbols correspond to the fit of hadron yield ratios with all the conservation laws (4)-(6) accounted for, while the larger symbols are obtained by the fit of hadron multiplicities, by ignoring Eq. (5) (see the text for details)

As is seen from Fig. 1, the experimental hadron yield ratios are reproduced very well within the present model. The dependence of the chemical freeze-out fitting parameters on $\sqrt{S_{NN}}$ is given in Fig. 2. In Fig. 2, we show only the statistical errors for the obtained fit; while, for the parameters of work [2], the shown errors account for the systematic and statistical ones. As one can see from Fig. 2, the discrepancy between the results of the present model and those of [2] is within the error bars.

Similarly to [2], we found that both the chemical freeze-out temperature T and the baryonic chemical potential μ_b are almost independent of the initial value of baryon charge $B_{\rm init}$ and the initial value of isospin projection $I_{3_{\rm init}}$. However, we found that the freeze-out volume V, which stands on the right-hand side of the conservation laws (5) and (6), is very sensitive to them. The obtained chemical freeze-out volume dependence on $\sqrt{S_{NN}}$ for $B_{\rm init} = 200$ and $I_{3_{\rm init}} = -20$ is shown in Fig. 3.

From the larger symbols in Fig. 3, one can clearly see that, for the center-of-mass collision energies $\sqrt{S_{NN}} = 2.7$–4.3 and $\sqrt{S_{NN}} = 12$–200 GeV, the found chemical freeze-out volume is so large that it exceeds the volume of kinetic freeze-out [9]. Here, we found that, unlike the hadron yield ratios, the chemical freeze-out volume is very sensitive both to the excluded volume correction and to the values of parameters $B_{\rm init}$ and $I_{3_{\rm init}}$. From Eq. (5), one can deduce that the larger value of excluded volume b corresponds to the larger value of chemical freeze-out volume V, since the larger the b value, the smaller the particle concentrations n_i and, consequently, the larger the volume $V = B_{\rm init}/\sum n_i B_i$. Therefore, the minimal chemical freeze-out volume corresponds to an ideal gas, i.e. for $b = 0$. This minimal chemical freeze-out

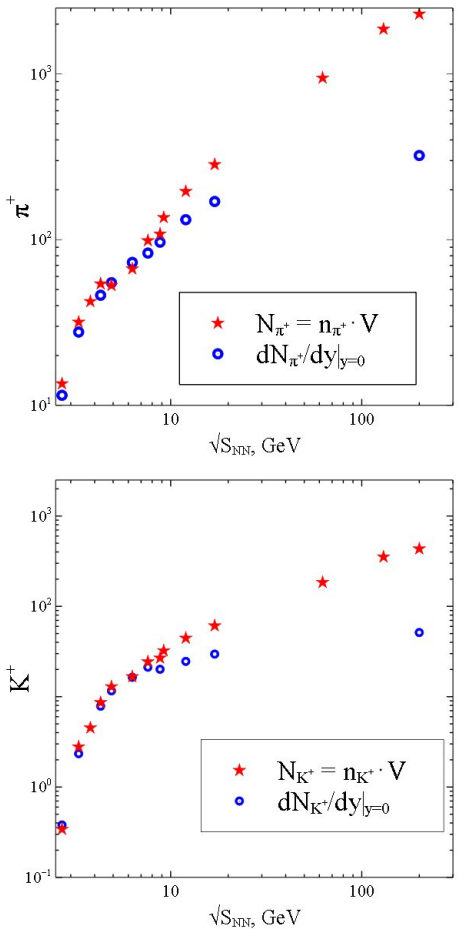

Fig. 4. Upper panel: π^+ multiplicity at chemical freeze-out vs. $\sqrt{S_{NN}}$. Lower panel: K^+ multiplicity at chemical freeze-out vs. $\sqrt{S_{NN}}$. The circles correspond to the experimental data, whereas the stars are found from particle densities as $N = nV$

volume is also shown in Fig. 3. Despite the absence of the excluded volume correction, the chemical freeze-out volume for an ideal gas remains huge. Hence, we conclude that the initial values in the conservation laws, namely $B_{\rm init}$ and $I_{3_{\rm init}}$, are of crucial importance for an extraction of the chemical freeze-out volume.

From the comparison of the hadron multiplicity $N = nV$ obtained within the thermal model and its experimental value $dN/dy|_{y=0}$ measured at zero rapidity, one can conclude whether the thermal model provides a reliable description of hadron multiplicities. Such a comparison for π^+ and K^+ mesons is shown in Fig. 4. Since the hadron yield ratios shown in Fig. 1 are described well by the thermal model, one would expect that, if the multiplicity of a single hadron type is in good agreement with the experimental data, then the multiplicities of all other sorts of hadrons should be well described too. However, from Fig. 4, one can see that, at $\sqrt{S_{NN}} \geq 10$ GeV, the experimental values of multiplicities are much smaller than the theoretical ones. At lower $\sqrt{S_{NN}}$, there is no such a problem, despite the big chemical freeze-out volume V. Our conclusion is that, for higher energies, the value of parameters $B_{\rm init}$ and $|I_{3_{\rm init}}|$ should be taken smaller than those for lower energies. In particular, according to Fig. 4 at $\sqrt{S_{NN}} = 200$ GeV, the values of $B_{\rm init}$ and $|I_{3_{\rm init}}|$ should be about 10 times smaller than those for the low-energy collisions.

A different way to describe the hadron multiplicities was used in [2]. The chemical freeze-out volume V was treated there as a free parameter. Let us show that such a treatment leads to a mathematical ambiguity. Consider the conservation laws (4)–(6) together with the following expression for the pressure in the system:

$$p = p^{id}(T, \mu_b, \mu_s, \mu_{I_3}) \exp\left(-\frac{p\, b}{T}\right). \qquad (10)$$

This system of equations for six unknowns, i.e. T, μ_b, μ_s, μ_{I_3}, V, and p, includes four equations. Hence, two unknowns should be treated as free fitting parameters. If, however, one treats three unknowns as free parameters, then one of the equations may be not satisfied, in general. More specifically, if T, μ_b, and V are the free fitting parameters, then the baryon charge conservation equation (5) may be broken down. To demonstrate this explicitly, we have considered the thermal model fit with three free parameters – T, μ_b and V – and ignored the baryon charge conservation equation (5); while the isospin projection conservation law (6) was used to find the chemical potential μ_{I_3}. After fitting the experimental hadron multiplicities $dN/dy|_{y=0}$ (not their ratios!) for the same energy range as before, we found the resulting baryonic charge as $S_b = V \sum_{i=1}^{N} n_i B_i$ summing up the densities n_i of all baryons and antibaryons multiplied by their baryonic charge B_i. Clearly, if Eq. (5) is satisfied, then this sum, S_b, should match the value of $B_{\rm init} = 200$. However, Fig. 5 demonstrates that Eq. (5) cannot be satisfied. Although the chemical freeze-out temperature and the baryonic chemical potential obtained by the fitting of hadron multiplicities

do not differ essentially from those found by the fit of hadron yield ratios (see open squares in Fig. 2), the freeze-out volumes obtained from the multiplicity fit are essentially smaller (see smaller symbols in Fig. 3) and more physically adequate for $\sqrt{S_{NN}} \geq 5$ GeV than those found from the fit of hadron yield ratios.

Additionally, we found that the values of $B_{\rm init}$ and $I_{3_{\rm init}}$ should strongly depend on the collision energy: at $\sqrt{S_{NN}} = 200$ GeV, they are about ten times smaller than those at the AGS energies. The hadron yield ratios are not sensitive to the values of $B_{\rm init}$ and $I_{3_{\rm init}}$. Hence, the baryon charge and I_3 conservation can be neglected for the description of hadron yield ratios. If, however, one supposes that $B_{\rm init} = {\rm const} > 0$ and $I_{3_{\rm init}} = {\rm const} > 0$, then the description of hadron multiplicities completely fails. Evidently, one can describe the hadron multiplicities by introducing the $\sqrt{S_{NN}}$ dependence of $B_{\rm init}$ and $I_{3_{\rm init}}$ values, if such dependences are known. Since such dependences are unknown, one has to ignore the baryon charge (5) and isospin projection (6) conservation laws and to fit the parameters T, μ_b, μ_{I_3}, and V to describe the hadron multiplicities or to fit the parameters T, μ_b, and μ_{I_3} in order to get the description of hadron yield ratios. Note, however, that the strangeness conservation law (4) does not create such problems, and, hence, it should be always obeyed.

4. Chemical Freeze-out Criteria and Adiabatic Chemical Hadron Production

The thermal model discussed above allows us to clarify the long standing question on the physically appropriate chemical freeze-out criterion which is widely discussed [22, 23]. The most popular chemical freeze-out criteria are (I) the constant value of the mean energy per hadron, $\langle E\rangle/\langle N\rangle \simeq 1.08$ GeV, (II) the constant value of the entropy density to the cube of the temperature, $s/T^3 \simeq 7$, and (III) the constant value of the total baryon and antibaryon density $n_B + n_{\bar{B}} \simeq 0.12{\rm fm}^{-3}$. Criterion (I) is believed to be more robust, while criteria (II) and (III) show a strong dependence on the hard-core radius value [23]. We have performed the analysis and found that criteria (II) and (III) are not obeyed at all, while the validity of criterion (I) depends essentially on the thermal model parametrization. The validity of these statements for criteria (I) and (II) are, respectively, demonstrated in the middle and upper panels

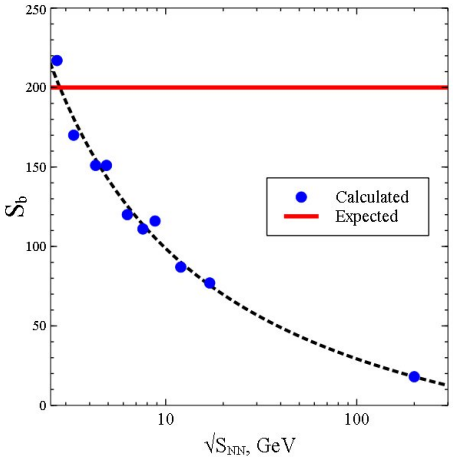

Fig. 5. Obtained baryonic charge $S_b = V\sum_{i=1}^{N} n_i B_i$ (dots) vs. $\sqrt{S_{NN}}$. The dots are calculated from the baryon charge conservation, whereas the line corresponds to the expected value $B_{\rm init} = 200$

of Fig. 6. Moreover, the thermal model results that we extracted from [2] are very similar to our ones, despite several differences in the parametrizations of these two models.

Our detailed analysis shows that there exists a much more robust chemical freeze-out criterion than all previously discussed ones. This novel criterion corresponds to the constant value of the entropy per number of particles which can be expressed in terms of the entropy density s and the hadron number density $\rho_{\rm part}$ as

$$\frac{s}{\rho_{\rm part}} \simeq 7.18. \qquad (11)$$

The lower panel of Fig. 6 shows that, for two different parametrizations of the thermal model, the ratio $\frac{s}{\rho_{\rm part}}$ stands between 6.6 and 7.6, i.e. it deviates within $\pm$ 8 % only, while the values of the center-of-mass energy of the collision change by two orders of magnitude! Such a behavior of the $\frac{s}{\rho_{\rm part}}$ quantity evidences for the *adiabatic chemical hadron production* in heavy ion collisions.

5. Multicomponent Gas and Hard-Core Radii

Although it is clear that the hadron radii can serve as the parameters of the thermal model, they, however, are rarely treated as free parameters. The common approach is to fix one radius for all hadrons. The value of this radius was discussed in [11], and it ranges

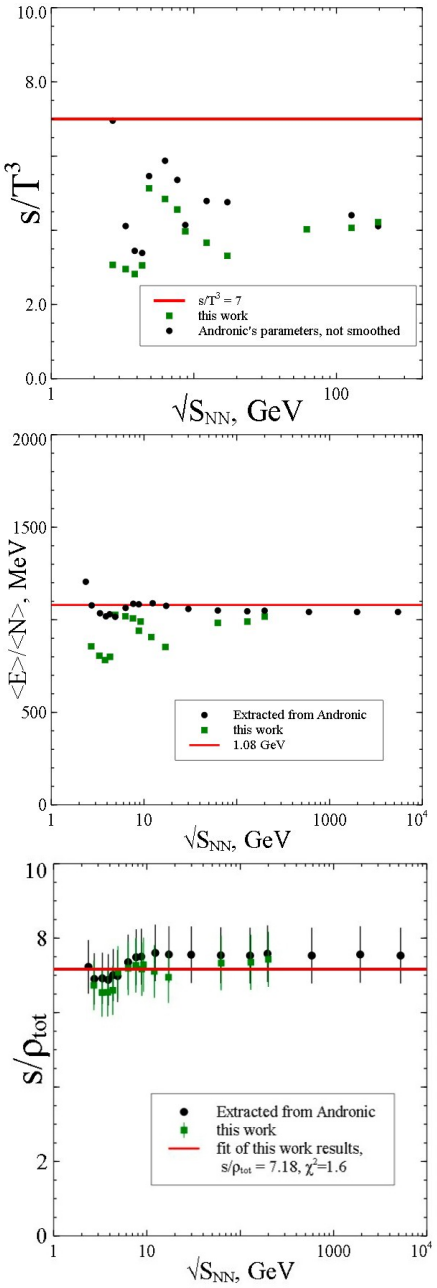

Fig. 6. Different chemical freeze-out criteria. Upper panel: the ratio of the entropy density to the cube of temperature s/T^3 at chemical freeze-out vs. $\sqrt{S_{NN}}$. Middle panel: the energy per particle $\langle E\rangle/\langle N\rangle$ at the chemical chemical freeze-out vs. $\sqrt{S_{NN}}$. Lower panel: the novel criterion of chemical freeze-out, entropy per particle at the chemical freeze-out $s/\rho \simeq 7.18$. The shown errors combine the statistical and systematic errors. The results of the present work (squares) are very similar to those extracted from [2]

from 0.2 fm to 0.8 fm [12]. However, the value $r = 0.3$ fm that was taken from the nucleon-nucleon scattering [10] seems to be an established value. To investigate the role of the hard-core radii, we introduce the different radii for mesons R_m and for baryons and R_b, respectively. To study the influence of the Lorentz contraction of hard-core radii on the chemical freeze-out parameters T and μ_b and on the hadron yield particle ratios, we need the hadron gas model, which accounts for different values of their eigenvolumes. For this purpose, we use the approach developed in [24, 25, 29]. Below, we give the necessary theoretical apparatus to study a multicomponent hadron gas mixture, whereas the results of the global fit for the cases with and without Lorentz contraction are given in the subsequent section.

Consider again the Boltzmann gas of s hadron species in a volume V at a temperature T. Let N_i be a quantity of the i-th sort of hadrons

$$N = \begin{pmatrix} N_1 \\ N_2 \\ \dots \\ N_s \end{pmatrix}. \tag{12}$$

The total number of particles is $M = \sum_{i=1}^{s} N_i$. It is assumed that, for every two sorts of hadrons i and j, there is the excluded volume b_{ij}. Then one can introduce the excluded volume matrix $B = (b_{ij})$. Naturally, it is supposed that the matrix B is symmetric, i.e. $b_{ij} = b_{ji}$.

The canonical partition function can be obtained by adding the particles of some eigenvolume one-by-one and considering all the corresponding excluded volumes of the previously added particles. Such an approximation was suggested in [25], and it gives the following expression for the canonical partition of a van der Waals hadron gas mixture

$$Z_{\rm VdW}(T,V,N_i) = \left[\prod_{i=1}^{s} \frac{\phi_i^{N_i}}{N_i!}\right] \left[V - \frac{N^T B N}{M}\right]^M, \tag{13}$$

where the thermal particle density $\phi_i(T,m,g)$ is defined in (3), and N^T is the transposed matrix to that one given by (12).

In the next step, we write the grand canonical partition function (GCPF) as

$$\mathcal{Z} = \sum_{N_1=1}^{\infty} \sum_{N_2=1}^{\infty} \dots \sum_{N_s=1}^{\infty} \left(\prod_{i=1}^{s} \exp\left[\frac{\mu_i N_i}{T}\right]\right) \times Z_{\rm VdW}. \tag{14}$$

It is well known [31] that, in the thermodynamic limit, the GCPF can be replaced by the maximal term of the multiple sum in $\mathcal{Z}$ (the maximum term method). Suppose that the array N^* gives the maximal term of $\mathcal{Z}$. Then the pressure in the system is given by

$$p/T = \lim_{V\to\infty} \frac{\mathcal{Z}}{V} = \\ = \lim_{V\to\infty} \frac{1}{V} \ln \left[\prod_{i=1}^{s} \frac{A_i^{N_i^*}}{N_i^*!} \left(V - \frac{(N^*)^T B N^*}{M^*} \right)^{M^*} \right], \quad (15)$$

where $A_i = \phi_i \exp\left[\frac{\mu_i}{T}\right]$. Let us find N^* from the maximum conditions ($i = 1..s$):

$$\frac{\partial}{\partial N_i^*} \left[\ln \left[\prod_{i=1}^{s} \frac{A_i^{N_i^*}}{N_i^*!} \left(V - \frac{(N^*)^T B N^*}{M^*} \right)^{M^*} \right] \right] = 0. \quad (16)$$

Performing the differentiations, we get

$$\xi_i = A_i \exp\left(- \sum_{j=1}^{s} 2\xi_j b_{ij} + \frac{\xi^T B \xi}{\sum_{j=1}^{s} \xi_j} \right), \quad (17)$$

with $\xi_i = \frac{N_i}{V - \frac{N^T B N}{M}}$ and

$$\xi = \begin{pmatrix} \xi_1 \\ \xi_2 \\ \dots \\ \xi_s \end{pmatrix}. \quad (18)$$

Using (17), one can express the hadron densities $n_i = \\ = \frac{N_i^*}{V}$ and the system pressure p as

$$n_i = \frac{\xi_i}{1 + \frac{\xi^T B \xi}{\sum_{j=1}^{s} \xi_j}}, \quad p = T \sum_{i=1}^{s} \xi_i. \quad (19)$$

The solution of the system of equations (17)–(19) defines the hadron densities for the multicomponent gas.

In a special case, if all the elements of the excluded volume matrix are equal $b_{ij} = v_0$, Eqs. (17)–(19) give

$$\begin{cases} \xi_i = A_i \exp(-p\, v_0/T), \\ n_i = \frac{\xi_i}{1 + p\, v_0/T}, \\ p/T = \left(\sum_{i=1}^{s} A_i\right) \exp(-p\, v_0/T). \end{cases} \quad (20)$$

In this case, the ratios of two-particle densities from (20) match those of the mixture of the corresponding ideal gases for an arbitrary value of v_0, while the particle densities themselves may essentially differ from the particle densities of the ideal gas.

6. Results for Hard-Core Radii with the Lorentz Contraction

In this section, it is assumed that all baryons have the same hard-core radius R_b, and all mesons have the same hard-core radius R_m. By performing the global fit, we would like firstly to find the pair of radii (R_m, R_b) that provides the best fit, and, secondly, we would like to study the influence of Lorentz contraction of the chemical freeze-out parameters.

To simplify the numerics, let us define that two hadrons belong to the same type, if their excluded volumes are equal. The number of equations in system (17) is equal to the number of particle types. Hence, the case with the Lorentz contraction included is more complicated, because, instead of two sets of particles, one should treat each hadron type as a new kind of particles. In order to avoid the large number of equations in system (17), the particles heavier than 900 MeV are considered non-relativistically, i.e. they all belong to two sorts: either to the baryons with the hard-core radius R_b or to heavy mesons with hard-core radius R_m. For two particles i and j, both heavier than 900 MeV, the element of the excluded volume matrix $b_{i,j}$ is $\frac{2\pi}{3}(R_i + R_j)^3$. For other cases, the second virial coefficients $b_{i,j}$ are calculated using Eqs. (3) and (4) of [29] by the direct translation of one ellipsoid around the other with the subsequent averaging of the obtained excluded volume over the ellipsoid positions.

The fit procedure is the same as that described in the preceding subsection: we fit the hadron yield ratios by T, μ_b, and V, respect the isospin projection conservation law (6) to find the value of μ_{I_3}, but ignore the baryonic charge conservation law (5). This effort to study the role of the Lorentz contraction is inspired by the fact that the conventional thermal model has problems with the description of light mesons. Thus, to describe the pion multiplicity and the ratios containing the pions, it was proposed to introduce R_π which is smaller than all the other hadron radii [5, 30]. Another example of difficulties with the light mesons is a "Strangeness Horn", i.e. the peak in the K^+/π^+ ratio. Its description was finally improved by fitting the $\sigma(600)$ meson mass and width [3], but the obtained description is far from being very good.

Let us see whether the Lorentz contraction might resolve these problems. At a given temperature,

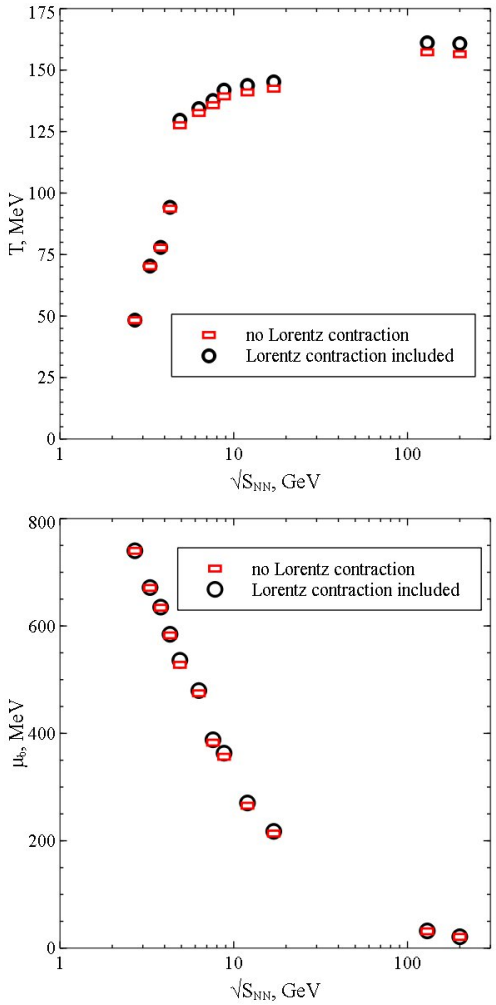

Fig. 7. The chemical freeze-out parameters obtained from the fit with (circles) and without (rectangles) the Lorentz contraction. Upper panel: the chemical freeze-out temperature T vs. $\sqrt{S_{NN}}$. Lower panel: the chemical freeze-out baryonic chemical potential μ_b vs. $\sqrt{S_{NN}}$

the eigenvolumes of the lighter particles decrease more than that of the heavier ones. Consequently, the excluded volume of lighter particles gets smaller compared to the excluded volume of heavier ones [24, 25, 29]. Such a behavior of the Lorentz contracted excluded volume provides us with the natural explanation of the fact that the pion hard-core radius R_π is smaller than other hard-core radii. On the other hand, this might improve the Strangeness Horn description. It was also shown [29] that the Lorentz contraction removes the causality paradox from the

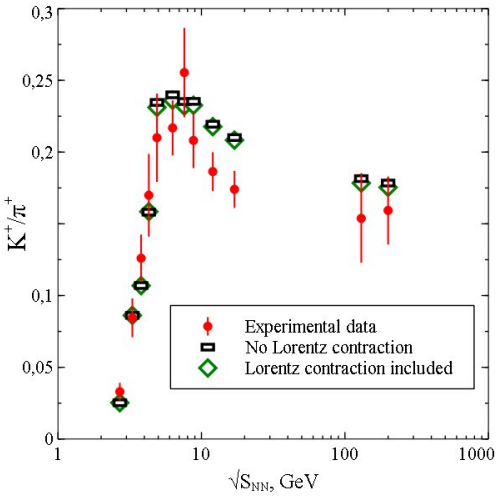

Fig. 8. Strangeness Horn description improvement for the model with the Lorentz contraction included and without it

thermal model, i.e. the speed of sound at high densities does not exceed the speed of light. Therefore, it is necessary to incorporate the Lorentz contraction into the conventional thermal model and to study its effect on the hadron multiplicity description. In order to make the numerical evaluation of the relativistic excluded volumes faster, we heuristically derived an approximate formula for such volumes, which allows one to reduce the six-dimensional integration over the pair of three-vectors of particle momenta to the three-dimensional integral. The derivation of such a formula and its verification are given in the Appendix.

To compare the models with and without the Lorentz contraction, we have chosen the hard-core radii $R_m = 0.45$ fm and $R_b = 0.3$ fm and have found the new best-fit T and μ_b values for the case with Lorentz contraction, see Fig. 7. From this figure, one can conclude that the baryo-chemical potential is almost unaffected by the Lorentz contraction, while the temperature is slightly higher for the case with the Lorentz contraction. It is also interesting to check, whether the inclusion of the Lorentz contraction improves the Strangeness Horn description. From Fig. 8, we conclude that there is a small improvement, which is not sufficient to qualitatively improve the Strangeness Horn description.

The important result, however, is that the Lorentz contraction inclusion provides us with the better fit quality for any pair of radii (R_m, R_b). From Fig. 9, one can see the difference between the χ^2/NDF val-

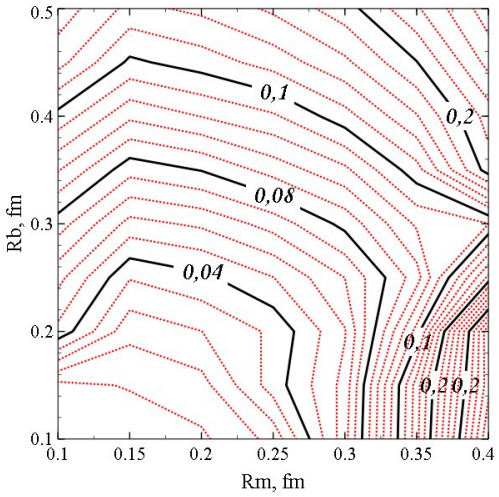

Fig. 9. Difference of χ^2/NDF between the model without the Lorentz contraction and the model with it for different values of meson and baryon hard-core radii

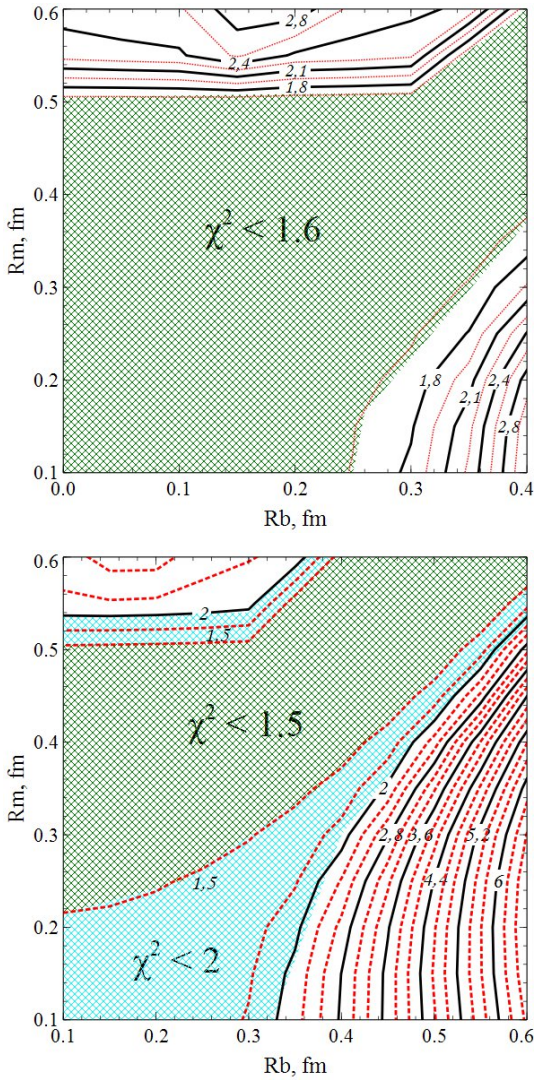

Fig. 10. Upper panel: χ^2/NDF for the model without the Lorentz contraction for different values of meson and baryon hard-core radii. Lower panel: same as in the upper panel, but for the model with the Lorentz contraction included

ues found without the Lorentz contraction and with it. Obviously, when both radii are small, then the correction due to the Lorentz contraction is small too. At $(R_b, R_m) = (0.3, 0.4)$ fm, $\Delta\chi^2/NDF \approx 0.1$, while χ^2/NDF itself is 1.48.

The simplest way to obtain the best fit radii is to perform a global fit, including the radii into the fitting procedure. However, in the (R_m, R_b) plane, there exist the domains, where χ^2 stays almost unchanged. For example, in the case without the Lorentz contraction, χ^2 is the same along the line $R_b = R_m$, which follows directly from (20). This makes the straightforward global fit rather difficult. Therefore, we perform the fit procedure of particle ratios in central nucleus-nucleus collisions at $\sqrt{S_{NN}} = 2.7$, 3.3, 3.8, 4.3, 4.9, 6.3, 7.6, 8.8, 12, 17, 130, 200 GeV for each pair of the radii (R_m, R_b) and find the domains, where χ^2 differs from its minimal value less than 10%. The results are shown in Fig. 10.

7. Determination of Hadronic Surface Tension

Recently the extremely important role of the surface tension of quark gluon bags was realized within the exactly solvable models for the deconfinement phase transition with the tricritical [32, 33] and the critical [34] endpoints. It was shown [32–34] that the (tri)critical endpoint appears due to vanishing the surface tension coefficient, while, at low baryonic densities, the deconfinement phase transition degenerates into a cross-over just due to the negative values of surface tension coefficient. The existence of the negative values of surface tension coefficient at the cross-over temperature was demonstrated analytically within the model of color confining tube [35]. Using this model, it was possible to predict the value of (tri)critical temperature of QCD phase diagram $T_{\rm cep} = 152.9 \pm 4.5$ MeV [36] using the plausible assumption on the temperature dependence of the sur-

Table 1. **Results of the global fit including the extracted surface tension parameters**

Collision energies set, $\sqrt{S_{NN}}$	χ^2/NDF without surface tension	χ^2/NDF with surface tension	σ_0, MeV fm^{-2}	T_0, MeV
2.7–7.6	25.8135/33 = 0.782	25.8043/31 = 0.832	0.91×10^{-2}	61
2.7–200	103.096/82 = 1.2573	103.036/80 = 1.288	-1.37×10^{-2}	57
2.7–62.4 (no 130 and 200)	85.51/65 = 1.3156	85.268/63 = 1.3534	-3.21×10^{-2}	62
12, 17, 62.4, 130, 200	62.5452/37 = 1.69	62.1454/35 = 1.776	0.654	147

face tension coefficient $\sigma(T) = a^2\left(1 - \frac{T}{T_{\rm cep}}\right)$ [37], which is typical of ordinary liquids.

Since the lattice QCD is not reliable at the non-zero values of the baryonic chemical potential, it would be interesting to study the surface tension for hadrons at the chemical freeze-out. The surface free energy can be written as $F_{\rm surf} = \sigma(T)S$, where the hadron surface S is given by its hard-core radius R as $S = 4\pi R^2$. Note that such a parametrization of the surface free energy is typical of multicomponent gas mixtures [32–34, 38]. Inclusion of the surface free energy into the thermal model is equivalent to adding the term $\sigma(T)S$ to the total chemical potential. If S is the same for all hadrons, such a surface tension correction does not affect the hadron yield ratios. Therefore, we have taken $R_m = 0.45$ fm, $R_b = 0.3$ fm, to have the noticeable radii difference. In the actual simulations, the surface tension coefficient $\sigma(T)$ was parametrized as

$$\sigma(T) = \sigma_0\left(1 - \frac{T}{T_0}\right). \qquad (21)$$

Here, σ_0 and $T_0 > 0$ are the free parameters to be found from a global fit. Note that, for $T \leq T_0$, such a temperature dependence coincides with the famous Fisher droplet model parametrization [37]; whereas, for $T > T_0$, it is in line with the recent findings [32–36]. We have performed several global fits with the parametrization (21), using different data sets. The results are listed in Table 1.

From this table, one can conclude that the inclusion of the surface tension in the form (21) does not improve the fit quality. However, since the value of χ^2/NDF in all cases is almost the same as that without accounting for the surface tension, it also does not spoil the fit quality. This fact allows us to take the obtained values of parameters σ_0 and T_0 rather seriously. It is not surprising that the value of σ_0 is close to zero; otherwise, the sizable surface tension of hadrons could be already found. The really surprising fact is that, for the center-of-mass energies $\sqrt{S_{NN}} \geq 12$ GeV, the parameter $T_0 = 147 \pm 7$ MeV is extremely close to the critical temperature value $T_{\rm cep} = 152.9 \pm 4.5$ MeV found in [36] more than a year ago using the entirely different approach. Of course, the reason of why the global fit that includes the low-energy data gives the essentially lower value of the parameter T_0 should be understood, and, hence, the investigation of the hadronic surface tension should be continued using both the experimental data on hadron production and the lattice QCD data.

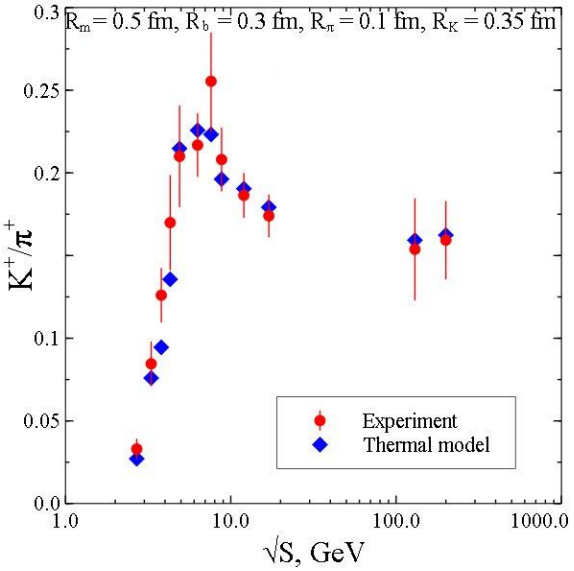

Fig. 11. Strangeness Horn description for the model with pion and kaon hard-core radii to be independent fitting parameters. The resulting quality of the global fit is $\chi^2/NDF \simeq 1.19$

8. Multicomponent Hadron Gas and the Strangeness Horn Description

The thorough analysis performed above led us to a conclusion that, besides the hadron surface tension inclusion, the further improvement of the thermal

model can be achieved, if we consider the pion and kaon hard-core radii, as independent fitting parameters. On the one hand, this would allow us to have two additional fitting parameters, and, on the other hand, one could include the Strangeness Horn data into the fitting procedure. Note that the quality of the Strangeness Horn description is far from being satisfactory up to now, although very different formulations of the thermal model are used for this purpose [2, 30, 39]. Thus, the most recent compilation of the Strangeness Horn description by the different thermal models can be found in [39].

The necessity to improve the Strangeness Horn description can be easily understood from the fact that just the non-monotonic behavior of the K^+/π^+ ratio as a function of the center-of-mass energy of collision is often claimed to be one of a few existing signals of the onset of a deconfinement [40–42]. The multicomponent hadron gas model developed in [25] is perfectly suited to treat the pion and kaon hard-core radii as independent fitting parameters. The physical idea behind such an approach is that the hadronic hard-core radii are the effective parameters, which include the contributions of repulsion and attraction. Since the parameters of the hadron-hadron interaction are, generally speaking, individual for each kind of hadrons, each kind of hadrons can have its own hard-core radius. Based on this idea, we performed a global fit of all hadron multiplicities (as described above) together with the Strangeness Horn data, by considering the pion hard-core radius R_π and the kaon hard-core radius R_K as independent variables together with the chemical freeze-out temperature and the baryonic chemical potential, whereas the hard-core radius of all other mesons and the hard-core radius of baryons were fixed, respectively, as $R_b = 0.3$ fm and $R_m = 0.5$ fm, according to the findings of Section 6.

The results of such a fit are shown in Fig. 11. Comparing Figs. 8 and 11, one can see the dramatic improvement of the K^+/π^+ ratio for the collision energies $\sqrt{S_{NN}}$ above 8 GeV. In fact, the K^+/π^+ ratio shown in Fig. 11 deviates from the experimental error bars only for the energy $\sqrt{S_{NN}} = 3.8$ GeV, while for all other collision energies it does not essentially deviate from the experimental error bars. Thus, the variations of the pion and kaon hard-core radii essentially improve the description of this ratio for all collision energies, but, at the same time, the quality of the fit of all other hadronic multiplicities does not worsen as it is seen from the resulting value of $\chi^2/NDF \simeq 1.19$ for the global fit, which, so far, is the best result obtained in the literature.

9. Conclusions

In this work, we performed a comprehensive analysis of the experimental hadron multiplicities within the thermal model. As in previous studies, the considered thermal model has two hard-core radii (R_b for baryons and R_m for mesons) and two new elements: an inclusion of the Lorentz contraction of eigenvolumes of hadrons and a treatment of the hadronic surface tension. Using this model, we studied the role of the imposed conservation laws (5) and (6) and showed that, for the adequate description of hadron multiplicities, the conservation laws should be modified, whereas, for the description of the hadron yield ratios, the conservation laws are not necessary at all. In addition, we suggested and analyzed the thermal model, in which the pion and kaon hard-core radii are independent fitting parameters compared to all other mesons.

Here, we also analyzed the usual criteria for the chemical freeze-out and found that none of them is robust. Therefore, we suggested a novel criterion of chemical freeze-out, a constant value of entropy per hadron number equal to 7.18. Such a criterion is also supported by different formulations of the thermal model [2], and it evidences for the new physical effect which we called the *adiabatic chemical hadron production*.

The performed analysis allowed us to find the restrictions on the hard-core radii that are imposed by the experimental data. We also showed that, although the inclusion of the Lorentz contraction improves the fit quality for any pair of baryon and meson hard-core radii, it has a small effect on the chemical freeze-out parameters and on K^+/π^+ ratio.

In addition, we phenomenologically introduced the surface tension in the thermal model and made several global fits to find its parameters. Although the surface tension inclusion does not improve the fit quality, it is found for the first time that the temperature of the nil surface tension value depends on the considered interval of the collision energy. Thus, if the low-energy data are included into the fit, then the nil surface tension temperature is about 60 ± 5 MeV, while the data for the center-of-mass energies

above 10 GeV lead to an essentially larger value of this temperature: $T_0 = 147 \pm 7$ MeV. The latter is a very intriguing result, since a very close estimate for the nil surface tension temperature was obtained recently within the entirely different analysis of the quark gluon bag surface tension [35]. Therefore, it is possible that these two independently obtained results, indeed, evidence that the (tri)critical temperature of the QCD phase diagram is between 140 and 154 MeV.

The most dramatic numerical effect, however, is obtained for the truly multicomponent hadron gas model worked out in [25] and employed here for the first time. In this model, the hard-core radii of pions and kaons differ from the hard-core radius of all other mesons, and they are treated as independent fitting parameters. Such an approach allowed us for the first time to simultaneously fit the hadron multiplicities together with the Strangeness Horn and to get the chemical freeze-out data description of a very high quality.

We would like to thank A. Andronic for providing an access to well-structured experimental data and A.I. Ivanytskyi, I.N. Mishustin, and L.M. Satarov for fruitful discussions. K.A.B. and D.R.O. acknowledge the partial support of the Program 'On Perspective Fundamental Research in High Energy and Nuclear Physics' launched by the Section of Nuclear Physics of the National Academy of Sciences of Ukraine. The work of A.S.S. was supported in part by the Russian Foundation for Basic Research, Grant No. 11-02-01538-a.

APPENDIX
Heuristic derivation of the approximate excluded volume formula for ellipsoids of revolution

In order to fasten the numerical evaluation of the relativistic excluded volumes, we would like to obtain an approximate expression, which would reduce the dimension of momentum integrations of two particles from six to three. Basically, we employ the heuristic method suggested in [29]. The main difference, however, is in that work [29] gives the ultra-relativistic expression for the excluded volume, while we would like to get an expression, which would be accurate both in the non-relativistic and ultra-relativistic limits.

For this purpose, let us consider two relativistic spheres S_1 and S_2, the γ-factors being γ_1 and γ_2, respectively. The hard-core radii in their rest frames are R_1 and R_2, respectively. Let us fix an angle θ between the momenta of two particles, which is the standard spherical angle. It is chosen in such a way that the three-momentum of S_1 coincides with the OZ-axis (see Figs. 12 and 13 for details). Then the angle θ is the azimuthal spherical angle of the momentum of the second particle. Due to the Lorentz contraction, the both spheres shrink in the direction of their momenta, and one obtains two ellipsoids of revolution. Here, we show how to get an approximate formula for the excluded volume for such ellipsoids.

The basic idea is to neglect the complexity of the problem and to treat the excluded volume as an ellipsoid, afterward to symmetrize the obtained expression with respect to the interchange $1 \leftrightarrow 2$, and to take a half of the sum of two expressions. Then the unsymmetrized excluded volume reads

$$V_{\rm exc} = \frac{4}{3}\pi R_x R_y R_z, \tag{22}$$

where the ellipsoid's radii R_x, R_y, and R_z are found from the geometrical consideration given below.

From Fig. 12, one can see that

$$R_y = R_1 + R_2. \tag{23}$$

To obtain the radius R_x, one should consider the ellipsoids depicted in Figs. 13–15. The radius R_z can be found analogously to the radius R_x from Fig. 16.

Let us show how one can get an expression for the radius R_x. A convenient projection and the notations are depicted in Figs. 13 and 14. From Fig. 14, one gets

$$R_x = R_1 + \Delta x. \tag{24}$$

Turning the reference frame to the main axes x_2 and y_2 of S_2 (see Fig. 15), one easily finds the coordinates of the touching point $K(x_0, y_0)$. The equation of S_2 for the principal axes shown in Fig. 15 reads

$$x_2^2 + y_2^2\gamma_2^2 = R_2^2. \tag{25}$$

The equation for a tangent to an ellipse shown in Fig. 15 is

$$\frac{dy_2}{dx_2} = -\frac{x_2}{\gamma_2^2 y_2} = \mathrm{tg}(\pi/2 - \theta). \tag{26}$$

Now solving (25) together with (26), one gets the touching point coordinates x_0 and y_0:

$$x_0 = -\frac{R_2\gamma_2 \,\mathrm{ctg}\,\theta}{\sqrt{1+\gamma_2^2\,\mathrm{ctg}^2\,\theta}}, \tag{27}$$

$$y_0 = \frac{R_2}{\gamma_2\sqrt{1+\gamma_2^2\,\mathrm{ctg}^2\,\theta}}. \tag{28}$$

Turning back from the (x_2,y_2)-coordinate system to the (x,y)-system, we obtain

$$\Delta x = |x_0\cos\theta - y_0\sin\theta| = \frac{R_2\sin\theta}{\gamma_2}\sqrt{1+\gamma_2^2\,\mathrm{ctg}^2\,\theta} \tag{29}$$

in accord with Figs. 14 and 15. Hence, we get

$$R_x = R_1 + \frac{R_2\sin\theta}{\gamma_2}\sqrt{1+\gamma_2^2\,\mathrm{ctg}^2\,\theta}. \tag{30}$$

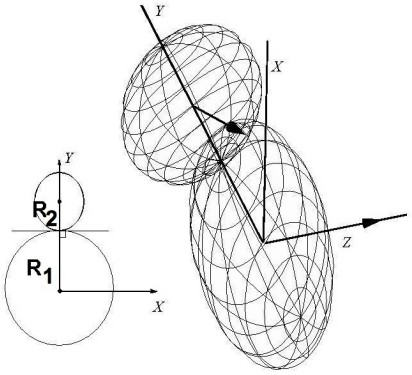

Fig. 12. Explanation of how to obtain the expression for the radius R_y of the relativistic excluded volume, when the second ellipsoid is translated around the first one in the plane XOY

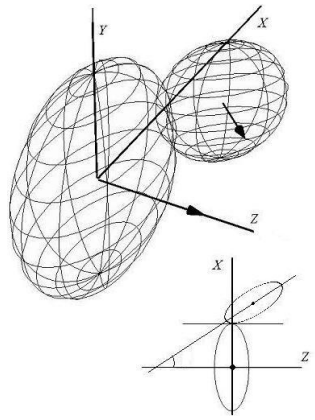

Fig. 13. Explanation of how to obtain the expression for the radius R_x of the relativistic excluded volume, when the second ellipsoid is translated around the first one in the plane XOZ

From Fig. 16, one can see that, in order to obtain the radius R_z, one should simply replace $R_1 \to R_1/\gamma_1$ and $\pi/2 - \theta \to \theta$ in expression (30) for the radius R_x. Then we find

$$R_z = \frac{R_1}{\gamma_1} + \frac{R_2 \cos\theta}{\gamma_2}\sqrt{1+\gamma_2^2\,\mathrm{tg}^2\,\theta}. \tag{31}$$

Finally, substituting Eqs. (23), (30), and (31) in (22), we obtain

$$V_{\mathrm{exc}} = \frac{4\pi}{3}(R_1+R_2)\left(\frac{R_1}{\gamma_1} + \frac{R_2\cos\theta}{\gamma_2}\sqrt{1+\gamma_2^2\,\mathrm{tg}^2\,\theta}\right)\times$$
$$\times\left(R_1 + \frac{R_2\sin\theta}{\gamma_2}\sqrt{1+\gamma_2^2\,\mathrm{ctg}^2\,\theta}\right). \tag{32}$$

Evidently, the expression above precisely recovers the excluded volume of two non-relativistic spheres, i.e. for $\gamma_1 = \gamma_2 = 1$. Thus, in contrast to the result of [29], Eq. (32) gives an exact result for the non-relativistic particles. One can analytically show that Eq. (32) gives a rather good approximation (with

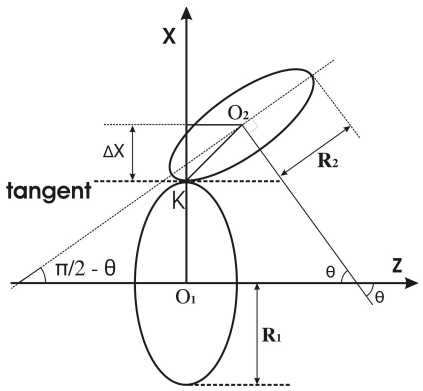

Fig. 14. Detailed projection of the second ellipsoid translation around the first one in the plane XOZ. This is the explanation of how to derive R_x from Fig. 13

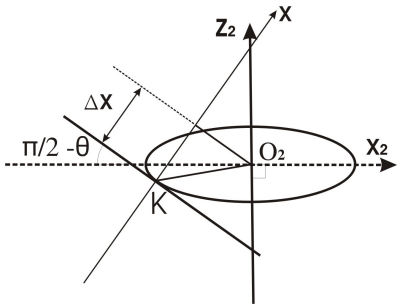

Fig. 15. Fragment of Fig. 14, which is necessary to determine the coordinates of the touching point K in the coordinate system of S_2

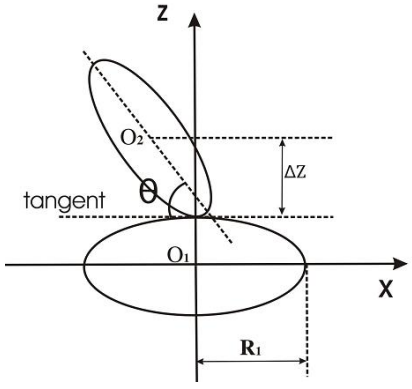

Fig. 16. Projection, which is necessary to derive the radius R_z of the approximate excluded volume (33). Comparing this projection with that shown in Fig. 14, we find that it is necessary to replace formally $R_1 \to R_1/\gamma_1$ and $\pi/2 - \theta \to \theta$ in expression (30) to get the expression for R_z from that for R_x

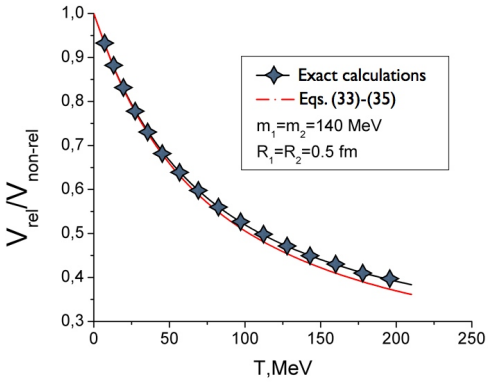

Fig. 17. Temperature dependence of the exact second virial coefficient of two pions (curve with symbols) and its approximation (curve without symbols) given by Eqs. (33)-(35) in the units of non-relativistic excluded volume $V_{\rm non-rel} = \frac{32}{3}\pi R_1^3$ of two hard spheres of the same radius $R_1 = R_2 = 0.5$ fm. The comparison is made for the pion-pion interaction only, since, in this case, the effect of Lorentz contraction is strongest

the deviation below 10 % from the exact result) also for other extreme cases where one particle is non-relativistic and another particle is ultra-relativistic or when both particles are ultra-relativistic.

Nevertheless, in order to improve (32) further, we symmetrize it with respect to the interchange $1 \leftrightarrow 2$. Evidently, such a procedure will not break down the above-discussed properties of (32). However, a symmetrization of (32) can be done in many possible ways, but we found numerically that the best approximation to an exact result is given by the expression

$$V_{\rm exc}^{\rm rel} = \frac{\pi}{12}(R_z + \tilde{R}_z)\left[(R_x + R_y)^2 + (\tilde{R}_x + \tilde{R}_y)^2\right], \qquad (33)$$

where the tilded values $\tilde{R}_a(R_1, R_2, \gamma_1, \gamma_2) = R_a(R_2, R_1, \gamma_2, \gamma_1)$ stand for the interchange $1 \leftrightarrow 2$ in the expressions for the radii R_x, R_y, and R_z of this Appendix. Expression (33) leads to the following approximate value of the second virial coefficient [29]:

$$V_{\rm rel} = \frac{1}{\rho(T, m_1)\rho(T, m_2)} \int \frac{d^3k_1}{(2\pi)^3}\frac{d^3k_2}{(2\pi)^3}\, V_{\rm exc}^{\rm rel}(k_1, k_2, \Theta_2) \times$$

$$\times \exp\left(-\frac{\sqrt{k_1^2 + m_1^2}}{T}\right) \exp\left(-\frac{\sqrt{k_2^2 + m_2^2}}{T}\right). \qquad (34)$$

Evidently, it can be analytically integrated over three spherical angles. In Eq. (34), the thermal density of the particle of mass m at temperature T is defined as

$$\rho(T, m) = \int \frac{d^3k_1}{(2\pi)^3} \exp\left(-\frac{\sqrt{k_1^2 + m^2}}{T}\right). \qquad (35)$$

A comparison between the exact value of the second virial coefficient with the Lorentz contraction accounted for both particles and the second virial coefficient found from approximation (33) is depicted in Fig. 17. For such a comparison, we choose the worst possible case, i.e. the largest allowed values of the hard-core radii, and take the pions, since the relativistic effects are most important for them. As one can see from Fig. 17, the approximate expression (33) gives a very good description of the pion-pion second virial coefficient. In fact, for temperatures below 180 MeV, the relative deviation of the obtained approximation does not exceed 6%. Since the hard-core repulsion provides a small correction (less than 10%) to the system pressure, the resulting error for the pion pressure generated by approximation (33) is less than 0.5% for all considered temperatures. The correction to the pressure of heavier hadrons is practically negligible, since the relativistic effects for them are essentially weaker than those for pions.

1. P. Braun-Munzinger, K. Redlich and J. Stachel, arXiv:0304013v1 [nucl-th] and references therein.
2. A. Andronic, P. Braun-Munzinger, and J. Stachel, Nucl. Phys. A **772**,167 (2006); arXiv:0511071v3 [nucl-th].
3. A. Andronic, P. Braun-Munzinger, and J. Stachel, arXiv:0812.1186v3 [nucl-th].
4. G.D. Yen and M.I. Gorenstein, Phys. Rev. C **59**, 2788 (1999).
5. G.D. Yen, M.I. Gorenstein, W. Greiner, and S.N. Yang, Phys. Rev. C **56**, 2210 (1997).
6. A. Andronic, P. Braun-Munzinger, J. Stachel, and M. Winn, arXiv:1201.0693v1 [nucl-th].
7. S. Wheaton and J. Cleymans, arXiv:0407174 [hep-ph].
8. L.M. Satarov, M.N. Dmitriev, and I.N. Mishustin, Phys. Atom. Nucl. **72**, 1390 (2009).
9. D. Adamova *et al.* (CERES collaboration), Phys. Rev. Lett. **90**, 022301 (2003); arXiv:0207008 [nucl-ex]; M. Lisa, S. Pratt, R. Soltz, and U. Wiedemann, Ann. Rev. Nucl. Part. Sci. **55**, 357 (2005); arXiv:0505014 [nucl-ex].
10. A. Bohr and B.R. Mottelson, *Nuclear Structure*, Vol. 1, (Benjamin, New York, 1969).
11. P. Braun-Munzinger, I. Heppe, and J. Stachel arXiv:9903010v2 [nucl-th].
12. G.D. Yen, M.I. Gorenstein, W. Greiner, and S.N. Yang, Phys. Rev. C **56**, 2210 (1997).
13. P. Braun-Munzinger, J. Stachel, J.P. Wesselsa, and N. Xu, Phys. Lett. B **344**, 43 (1995); arXiv:9410026 [nucl-th]; Phys. Lett. B **365**, 1 (1996); arXiv:9508020 [nucl-th].
14. J. Cleymans, D. Elliott, A. Keranen, and E. Suhonen, Phys. Rev. C **57**, 3319 (1998); arXiv:9711066 [nucl-th]; J. Cleymans, H. Oeschler, and K. Redlich, Phys. Rev. C **59**, 1663 (1999); arXiv:809027 [nucl-th].
15. R. Averbeck, R. Holzmann, V. Metag, and R.S. Simon, Phys. Rev. C **67**, 024903 (2003); arXiv:0012007 [nucl-ex].

16. P. Braun-Munzinger, I. Heppe, and J. Stachel, Phys. Lett. B **465**, 15 (1999); arXiv:9903010 [nucl-th].
17. P. Braun-Munzinger, D. Magestro, K. Redlich, and J. Stachel, Phys. Lett. B **518**, 41 (2001); arXiv:0105229 [nucl-th].
18. W. Broniowski, W. Florkowski, and M. Michalec, Acta Phys. Polon. B **33**, 761 (2002); arXiv:0106009 [nucl-th]; W. Broniowski and W. Florkowski, Phys. Rev. C **65**, 064905 (2002); arXiv:0112043 [nucl-th].
19. M. Kaneta and N. Xu, arXiv:0405068 [nucl-th].
20. J. Adams *et al.* (STAR collaboration), Nucl. Phys. A **757**, 102 (2005); arXiv:0501009 [nucl-ex].
21. R. Preghenella, arXiv:1111.7080 [hep-ex].
22. P. Braun-Munzinger and J. Stachel, Nucl. Phys. A **638**, 3c (1998); arXiv:9803015 [nucl-ex].
23. J. Cleymans and K. Redlich, Phys. Rev. Lett. **81**, 5284 (1998), **C 60**, 054908 (1999); J. Cleymans, H. Oeschler, K. Redlich, and S. Wheaton, Phys. Rev. **C 73**, 034905 (2006), J. Phys. **G 32**, S165 (2006).
24. K.A. Bugaev, M.I. Gorenstein, H. Stöcker, and W. Greiner, Phys. Lett. B **485**, 121 (2000).
25. G. Zeeb, K.A. Bugaev, P.T. Reuter, and H. Stöcker, Ukr. J. Phys. **53**, 279 (2008).
26. F. Becattini, M. Gazdzicki, A. Keranen, J. Manninen, and R. Stock, Phys. Rev. C **69**, 024905 (2004).
27. A. Dumitru, L. Portugal, and D. Zschiesche, Phys. Rev. C **73**, 024902 (2006); arXiv:0511084 [nucl-th].
28. K.A. Bugaev, V.K. Petrov, and G.M. Zinovjev, Europhys. Lett. **85**, 22002 (2009); arXiv:0801.4869v2 [hep-ph] and references therein.
29. K.A. Bugaev, Nucl. Phys. A **807**, 251 (2008); arXiv:1012.3400 [nucl-th].
30. R.A. Ritchie, M.I. Gorenstein, and H.G. Miller, Z. Phys. C **75** 2002 (1997).
31. R.K. Pathria, *Statistical Mechanics* (Pergamon Press, Oxford, 1972).
32. K.A. Bugaev, Phys. Rev. C **76**, 014903 (2007); Phys. Atom. Nucl. **71**, 1615 (2008);
33. A.I. Ivanytskyi, Nucl. Phys. A **880**, 12 (2012).
34. K.A. Bugaev, V.K. Petrov, and G.M. Zinovjev, Phys. Part. Nucl. Lett. **9**, 397 (2012).
35. K.A. Bugaev and G.M. Zinovjev, Nucl. Phys. A **848**, 443 (2010); K.A. Bugaev, Phys. Part. Nucl. Lett. **8**, 907 (2011).
36. K.A. Bugaev, A.I. Ivanytskyi, E.G. Nikonov, V.K. Petrov, A.S. Sorin, and G.M. Zinovjev, Phys. Atom. Nucl. **75**, 1 (2012).
37. M.E. Fisher, Physics **3**, 255 (1967).
38. K.A. Bugaev, M.I. Gorenstein, I. N. Mishustin, and W. Greiner, Phys. Rev. C **62**, 044320 (2000); Phys. Lett. B **498**, 144 (2001).
39. S.K. Tiwari, P.K. Srivastava, and C.P. Singh, Phys. Rev. C **85**, 014908 (2012).
40. M. Gazdzicki and M.I. Gorenstein, Acta Phys. Polon. B **30**, 2705 (1999).
41. M.I. Gorenstein, M. Gazdzicki, and K.A. Bugaev, Phys. Lett. B **567**, 175 (2003).
42. M. Gazdzicki, M.I. Gorenstein, and P. Seyboth, Acta Phys. Polon. B **42**, 307 (2011).

Received 14.08.12

Д.Р. Олійниченко, К.О. Бугаєв, О.С. Сорін

ДОСЛІДЖЕННЯ АДРОННИХ МНОЖИННОСТЕЙ І ВІДНОШЕНЬ ВИХОДІВ АДРОНІВ У ЗІТКНЕННЯХ ВАЖКИХ ІОНІВ

Р е з ю м е

У цій роботі докладно обмірковуються деякі слабкі сторони термальної моделі, яка традиційно використовується для опису адронних множинностей, які було виміряно в центральних ядро-ядерних зіткненнях. Зокрема, систематично досліджуються роль законів збереження, величини радіусів твердого кора адронів разом з ефектами лоренцова скорочення їх власних об'ємів і з поверхневим натягом адронів. Показано, що для адекватного опису адронних множинностей закони збереження повинні бути модифіковані, в той час як для опису відношень виходів частинок закони збереження взагалі не потрібні. Також проаналізовано звичайні критерії хімічного фрізаута і виявилось, що жоден із цих критеріїв не є строгим. Запропоновано новий критерій хімічного фрізаута сталої ентропії на частинку і обмірковано новий ефект адіабатичного народження адронів. Також знайдено, що дані для енергій зіткнення в системі центра мас вище за 10 ГеВ приводять до температури занулення коефіцієнта поверхневого натягу адронів $T_0 = 147 \pm 7$ МеВ. Це дуже інтригуючий результат, оскільки дуже близьку оцінку для цієї температури було отримано нещодавно за допомогою зовсім іншого підходу. Представлено аргументи на користь того, що ці два незалежно отримані результати свідчать про те, що значення (три)критичної температури фазової діаграми КХД знаходиться між 140 і 154 МеВ. Також в цій роботі запропоновано розглядати радіуси твердого кора піонів і каонів як нові параметри фітування. Такий підхід вперше дозволив одночасно описати як адронні множинності, так і Пік дивності і отримати високоякісний фіт наявних експериментальних даних.